Probing the Transverse Coherence of an Undulator X-Ray Beam Using Brownian Particles

M. D. Alaimo,[1,2] M. A. C. Potenza,[1] M. Manfredda,[1] G. Geloni,[3] M. Sztucki,[2] T. Narayanan,[2,*] and M. Giglio[1,*]

[1]*Dipartimento di Fisica, Università di Milano, I-20133 Milano, CNISM, Italy*
[2]*European Synchrotron Radiation Facility, BP-220, F-38043 Grenoble, France*
[3]*Deutsches Elektronen-Synchrotron and European XFEL GmbH, D-22607 Hamburg, Germany*

(Received 16 August 2009; published 5 November 2009)

We present a novel method to map the two-dimensional transverse coherence of an x-ray beam using the dynamical near-field speckles formed by scattering from colloidal particles. Owing to the statistical nature of the method, the coherence properties of synchrotron radiation from an undulator source is obtained with high accuracy. The two-dimensional complex coherence function is determined at the sample position and the imaging optical scheme further allowed us to evaluate the coherence factor at the undulator output despite the aberrations introduced by the focusing optics.

DOI: 10.1103/PhysRevLett.103.194805 PACS numbers: 41.50.+h, 07.85.Qe, 42.25.Kb, 61.05.cf

The development of high brilliance x-ray sources has generated great interest in coherence based methods that have already been successfully tested in the optical region. This includes intensity fluctuation spectroscopy (IFS), phase contrast imaging, holography, etc. [1]. Knowledge of the beam spatial coherence is a necessity both for the appropriate planning of experiments and data reduction. Quantitative experimental characterization of the spatial coherence at two points is determined by the quality of fringe patterns generated by the interference of radiation from these two points, the classical arrangement being Young's double-slit straight fringe method [2,3]. X-ray coherence measurements have already been performed with similar interference schemes which require specially fabricated optical elements [4–8] though simpler diffraction studies with a single aperture or obstruction have also been used [9,10].

Here, we present a method for measuring the two-dimensional spatial coherence by exploiting the circular fringes that are generated by the interference between perfectly spherical scattered waves from a colloidal suspension and the transmitted partially coherent beam observed at a distance from the sample. The superposition of many of these interference patterns leads to a speckle intensity distribution. If these speckles are recorded in the near-field region [11–14], the square root of the two-dimensional power spatial frequency spectrum yields the two-dimensional distribution of the modulus of the complex coherence factor (CCF), spatially averaged over the scatterer positions. Furthermore, the imaging optical geometry allowed us to estimate the dimension of the coherence areas at the source. We found that the strongly elongated source is nearly incoherent in the horizontal direction, but almost coherent in the vertical direction.

The colloidal sample consisted of silica spheres of diameter 450 nm with a narrow size distribution ($<5\%$) suspended in water (volume fraction ~ 0.06, without significant interactions) contained in a 2 mm diameter capillary. As the particles are executing Brownian motions, the interference fringes change, and consequently the speckles fluctuate. The advantages of using a dynamic sample are enormous, as time delayed image differences can be analyzed, and any static stray signal due to imperfections of optics is erased. Equally important is the accumulation of many statistical images, which leads to the great finesse typical of statistical methods like IFS.

The method was tested at a high brilliance undulator beam line ID02 (ESRF, Grenoble) [15]. The source (two undulators of period 21.4 mm and gap 11 mm) is nominally 19 μm in vertical and 950 μm in horizontal (full-width at half maximum values). A channel-cut Si(111) monochromator at 30 m from the source selects the fundamental wavelength (λ) of 0.1 nm with a bandwidth $\Delta\lambda/\lambda \approx 10^{-4}$. The focusing toroidal mirror is situated at 33 m

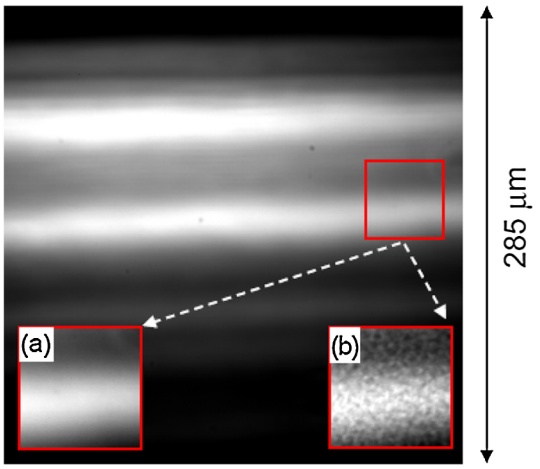

FIG. 1 (color online). The direct image of the beam depicting two brighter stripes which are distorted images of the undulator source. The mean square width of the intensity distribution is ~ 100 μm which is comparable with the calculated value by ray tracing (~ 90 μm). The beam profile appears roughly as a Gaussian with usual SAXS detector resolution (~ 60 μm). Insets (a) and (b) display magnified regions of the beam without and with colloidal particles, respectively.

from the source, and the beam is collimated by primary and secondary slits (with square apertures of 400×400 μm^2 and 300×300 μm^2, respectively) at distances of 27 m and 49.5 m from the source. The detector (FReLoN CCD camera with a conversion phosphor coupled to a microscope objective of magnification 50 corresponding to an effective pixel size ≈ 0.28 μm) was placed at 52.5 m and the scattering sample was placed at various distances z from the sensor (5 mm $< z <$ 250 mm).

Figure 1 presents the image as acquired from the sensor without the sample in place. The beam profile appears as a stack of (distorted) images of 40 μm high with most of the beam power falling in the two brighter patches. Classical statistical optics predicts that a snapshot with an exposure short compared to the reciprocal of the beam linewidth would capture the speckled image of the source, and the statistical properties of the field could be established by the analysis of these speckles. However, such extremely short exposures cannot be implemented experimentally. Here we demonstrate that this problem can be circumvented and obtain diffraction-limited information. Since the monochromator bandwidth is much smaller than the on-axis undulator bandwidth and much larger than the inverse bunch duration, radiation is quasimonochromatic, and the process is quasistationary. Thus, the method can be based on the classical definition of CCF and the interference law for stationary fields [3,16]:

$$\mu(P_0, P_1) = \langle E(P_0)E^*(P_1)\rangle / \sqrt{\langle I(P_0)\rangle \langle I(P_1)\rangle}, \quad (1)$$

where E and I are the amplitude and intensity of spherical waves at points P_0 and P_1. Its modulus is strictly related to the fringe visibility (V), that can be introduced in terms of the intensities of the two waves at the observation points, I_0 and I_1 [16]:

$$V = 2|\mu(P_0, P_1)| \sqrt{\langle I_0\rangle \langle I_1\rangle} / (\langle I_0\rangle + \langle I_1\rangle). \quad (2)$$

Figure 2 depicts the conceptual scheme of the method

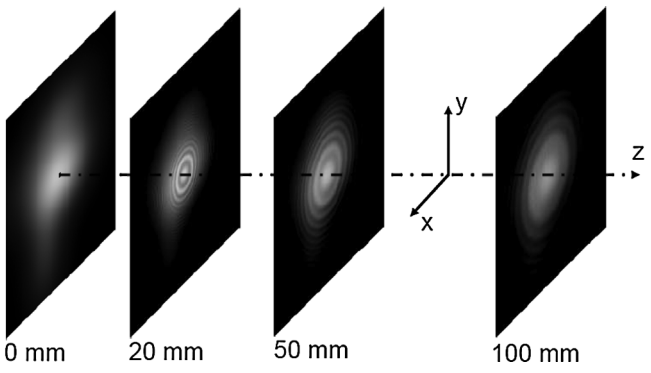

FIG. 2. Simulation of the interference patterns between a spherical wave ($\lambda = 1$ Å) and a single coherent patch of beam with limited transverse coherence. The size of the coherence patch at the origin ($z = 0$) is approximately 8 μm in diameter.

based on quantitative simulations using the parameter values indicated. The wave front from a partially coherent source can be considered as composed of adjoining coherent patches over which phase and amplitude are stationary. These patches are extremely short lived, they change shape and position, and the averages in Eq. (1) imply averaging over many patch lifetimes. In the present scheme, the interference is between one (weak) spherical scattered wave and the (strong) transmitted coherent patch wave. A scattered wave originated at P_0 by the coherent patch interferes with the same coherent patch at the displaced point P_1. The optical scheme is reminiscent of the point diffraction interferometer scheme (PDI) [5,6,17]. Since V changes with r, the distance between P_0 and P_1, the relevant parameter is $r = q/kz$. Where $\mathbf{q}$ is the scattering wave vector with magnitude, $q \sim 2k \sin(\theta/2) \sim k\theta$ (with θ the scattering angle and $k = 2\pi/\lambda$). The direct relation between r and q holds good because we are in the near-field regime corresponding to $z\theta < a$, the average size of the coherent patches [11,13]. Figure 2 also shows how V could, in principle, be measured in this ideal, one particle setup. As z is varied, the fringe pattern also changes and at a given position the fringe intensity oscillates. Once values of I_0 and I_1 are estimated, V can be derived after proper normalization.

Experimentally, single-particle scattering is not practical and a colloidal suspension is used. Therefore, many randomly staggered interference patterns are added up leading to a speckle intensity distribution. Insets of Fig. 1 show two enlarged views of a small region of the beam. When the sample is in place, tiny well-defined speckles float over the direct beam image. Over time, they move in a disordered manner typical of the laser light scattered from Brownian particles. Below we present how transverse coherence can be determined from the speckle analysis.

Quantitative characterization of speckle statistics is best done via intensity power spectra analysis. While the information about the fringe centers is lost, the method yields the mean square value of fluctuations around a chosen scattering wave vector, $\mathbf{q}$. An azimuthally averaged power spectrum $S(q)$ as a function of q (for $z = 68$ mm) is depicted in Fig. 3. If we had a perfect detector with flat transfer function, so that each interference pattern would have an infinite number of fringes with the same amplitude, the power spectrum would then coincides with the Talbot function $T(q) = \sin^2(q^2 z/2k)$ [12]. The amplitude of the Talbot oscillations decays because of multiple reasons, the limited spatial coherence being one.

The field scattered by the sample, e_s, interferes with the unperturbed transmitted field, e_0. The phosphor placed at a distance z from the sample records a signal $f(\boldsymbol{x}, z, t)$ which can be expressed as

$$f(\mathbf{x}, z, t) = \alpha\{i_0(\mathbf{x}) + 2\mathrm{Re}[e_0^*(\mathbf{x}) e_s(\mathbf{x}, z, t)]\} \otimes p(\mathbf{x}) + k(\mathbf{x}, t), \quad (3)$$

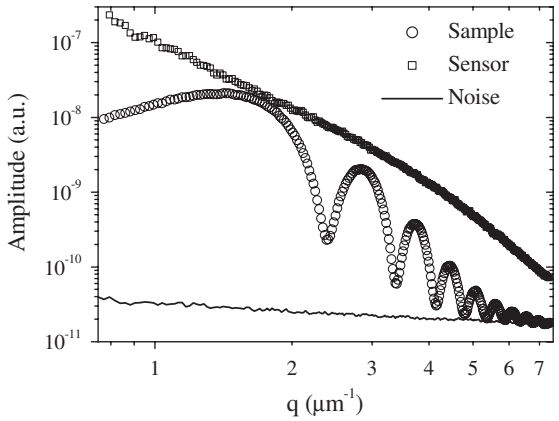

FIG. 3. Azimuthally averaged power spectra of the speckle intensity distribution generated by the colloidal suspension recorded at $z = 68$ mm, sensor power transfer function, and cumulative shot and readout noise.

where α is a constant depending on the sensor, $i_0(\mathbf{x}) = |e_0(\mathbf{x})|^2$ is the time-independent intensity of the strong transmitted field which includes also stray light, $p(\boldsymbol{x})$ is the sensor point spread function and $k(\boldsymbol{x}, t)$ is a fluctuating term due to shot noise and camera readout noise. Since the scattered field is much weaker than the transmitted one ($|e_s| \ll |e_0|$) the term $e_s^* e_s$ has been neglected. If $f(\boldsymbol{x}, z, t)$ and $f(\boldsymbol{x}, z, t + \tau)$ are two signals acquired with a time delay τ, the normalized difference signal is defined by

$$s(\mathbf{x}, z, \tau) \equiv \frac{f(\mathbf{x}, z, t) - f(\mathbf{x}, z, t + \tau)}{f(\mathbf{x}, z, t) + f(\mathbf{x}, z, t + \tau)} \sim \{\mathrm{Re}[e_s(\mathbf{x}, z, t) - e_s(\mathbf{x}, z, t + \tau)]\} \otimes p(\mathbf{x}) + k(\mathbf{x}, t) - k(\mathbf{x}, t + \tau), \quad (4)$$

which is not dependent on i_0. The time averaged two-dimensional Fourier power spectrum is given by [18]

$$S(\mathbf{q}, z, \tau) \equiv \langle |F\{s(\mathbf{x}, z, \tau)\}|^2 \rangle_t \sim [I(\mathbf{q})T(\mathbf{q}, z) - G(\mathbf{q}, \tau)]C(\mathbf{q}, z)P(\mathbf{q}) + K(\mathbf{q}), \quad (5)$$

where F is the Fourier transform operator, $G(\mathbf{q}, \tau)$ is the Fourier transform of the field-field correlation function, $P(\mathbf{q}) = |F[p(\mathbf{x})]|^2$ is the sensor transfer function, and $K(\mathbf{q}) = \langle |F[k(\mathbf{x}, t)]|^2 \rangle_t$ is the power spectrum of $k(\boldsymbol{x}, t)$. Complete decorrelation between speckle images ($G(\mathbf{q}, \tau) = 0$) is brought about by both diffusion and convective motions. Typically a delay time, τ of 2 sec brings decorrelation even at the lowest q vectors, mostly because of convective motions. Equation (5) is the square of the field relation used in phase contrast imaging [19] and the shadowgraphy in the optical region [20]. $I(q)$ is the power spectrum of the radiation scattered by the colloidal particles (almost flat) and $C(q) = |\mu|^2$, where $C(q) = C(r(q))$ with q introduced via the $r = q/kz$ relation, and it can be shown that this is a consequence of the "near-field" condition. $C(q)$ is the function we want to evaluate quantitatively. $P(q)$ can be determined according to the method outlined in Ref. [14] that for the present setup is shown in Fig. 3 (squares). The first step in data reduction is the subtraction of the noise term, $K(\mathbf{q})$, which was determined by taking power spectra of the signal for a cell filled with water (continuous line in Fig. 3).

The raw power spectrum, $S(q)$ spans over more than three decades, but almost 99% of the decay is due to the sensor response alone. This underlines the extreme accuracy and stability of the raw data, typically a few parts in 10^4. The influence of Talbot oscillations which modulate between 0 and 1 can be eliminated by plotting the data as a function of r. The value of $C(q)T(q)$ oscillates between zero and $T(q)$ at a given r due to contributions from different z. By plotting the maxima of these oscillations, we can generate the curves for the visibility V, a method that has also been used by Pfeiffer *et al.* [7]. V along the vertical (curve a) and horizontal (curve b) directions are shown in Fig. 4 and the inset displays a two-dimensional plot. The width in the horizontal direction is roughly 5 μm, and oscillations are fairly pronounced and show a sequence of minima typical of a diffraction pattern from a slit. Whereas in the vertical direction the modulations are weaker and have the typical minima structure of an interference pattern.

As we are dealing with fully developed speckles where the circular Gaussian statistics holds, the optical aberrations do not modify the speckle size [21]. If no slits were present, we would have measured the transverse coherence properties of the source around the optical axis in both horizontal and vertical directions. The horizontal coher-

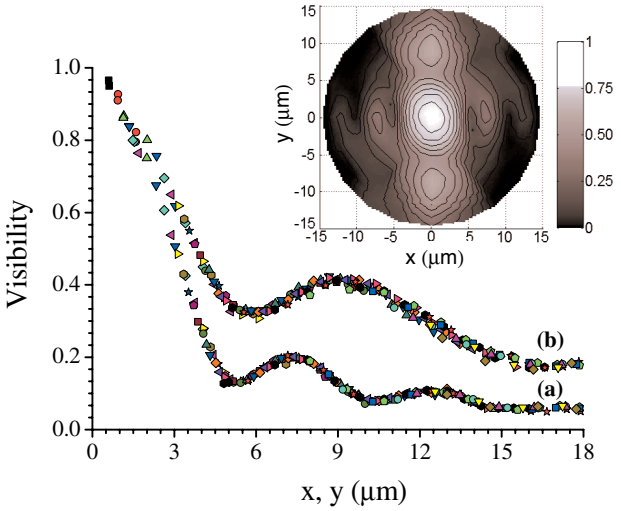

FIG. 4 (color online). Modulus of complex coherence factor (visibility) as a function of transverse displacements x and y represented by curves (a) and (b), respectively. These two curves are obtained from a stack of power spectra taken at various distances (5 mm $< z <$ 250 mm) denoted by different symbols and represent the maxima of the oscillating Talbot function. Inset shows the full two-dimensional distribution.

ence length at the source is related to the rms electron bunch divergence $\sigma'_x = 10.7$ μrad by inverse proportionality. Because of the small vertical emittance of the electron bunch, the vertical coherence length is related [22] both to the rms electron bunch divergence $\sigma'_y = 3.2$ μrad and to the single-particle diffraction-limited divergence, which are of the same magnitude. If we take into account the acceptance angle determined by the slits $\Theta_A = 16$ μrad, and compare it with the horizontal and vertical FWHM divergence of the electron beam, it turns out that the measurement of the coherence properties at the sensor site are influenced by the presence of the slit in the horizontal, but not in the vertical direction, where the divergence is smaller. This means that the horizontal speckle size, of the order of $a_x = 5$ μm, carries information on the slits acceptance angle only. Whereas in the vertical direction, the source has an average coherent patch at its output front, whose dimensions can be determined by the magnification ratio $m = 0.6$ and the observed vertical size of speckle at the sensor surface, $a_y = 8$ μm. It follows that at the source the coherent patch is about 13.6 μm. This number compares fairly well with expectations from an idealized model, where calculations are made at resonance for a single 3 m-long undulator with minimal betatron function at its center [22]. The above results show that the size of the coherent patch is similar to the source size in the vertical but significantly smaller in the horizontal direction.

The oscillations in the vertical section can be tentatively assigned to the presence of multiple images in the vertical direction (Fig. 1) corresponding to an apparent double source angle of 4 μrad. A rough estimate suggests that these oscillations are due to an interference between waves angularly separated by 4 μrad, and the position of the minima are compatible with the observed pattern. Note that the vertical coherence length at the source is of the order of the horizontal coherence length estimated from theory. This seems paradoxical, because of the tiny vertical emittance of the electron beam compared to the horizontal one. However, measurements have been done with a high β section, where the electron bunch divergence in the vertical direction is only a factor 3.3 smaller than in the horizontal. We found the experimental evidence for this nontrivial character of the spectral degree of coherence of the source in the vertical direction. Since measurements cannot be performed very close to the undulator (the closest distance at ESRF is 27 m), the use of imaging optics is essential as in this work. Equally important is the fact that speckle size determination is independent of aberrations and consequently, the measure of a_y yields a direct estimate of the coherence length at the source.

Finally, we emphasize that the near-field speckle method can be applied for any narrowband source, but in the case of wide spectral band, both spatial and temporal coherence contribute to the shaping of the two-dimensional visibility plot. Furthermore, the presented scheme is capable of detecting subtle time dependent coherence instabilities that cannot be evidenced with traditional beam monitoring methods. While such instabilities may not significantly affect the performance of traditional techniques like low angle static scattering or even IFS, they can have undesirable consequences in coherent imaging methods. Our approach is of interest for routine monitoring of coherence properties as well as shot to shot analysis of FEL beams.

The ESRF is acknowledged for the provision of synchrotron beam time and financial support. J. Gorini and P. Van Vaerenbergh are thanked for technical assistance. Discussions with N. Piovella are gratefully acknowledged.

*narayan@esrf.fr
marzio.giglio@unimi.it

[1] *Third Generation Hard X-Ray Synchrotron Radiation Sources*, edited by D. Mills (John Wiley and Sons, Inc., New York, 2002).
[2] B. J. Thompson and E. Wolf, J. Opt. Soc. Am. **47**, 895 (1957).
[3] M. Born and E. Wolf, *Principles of Optics* (Cambridge University Press, Cambridge, England, 1999).
[4] J. J. A. Lin *et al.*, Phys. Rev. Lett. **90**, 074801 (2003).
[5] W. Leitenberger *et al.*, J. Synchrotron Radiat. **11**, 190 (2004).
[6] U. Pietsch *et al.*, Physica (Amsterdam) **357B**, 45 (2005).
[7] F. Pfeiffer *et al.*, Phys. Rev. Lett. **94**, 164801 (2005).
[8] A. Snigirev *et al.*, Phys. Rev. Lett. **103**, 064801 (2009).
[9] A. Snigirev *et al.*, Rev. Sci. Instrum. **66**, 5486 (1995).
[10] V. Kohn, I. Snigireva, and A. Snigirev, Phys. Rev. Lett. **85**, 2745 (2000).
[11] M. Giglio, M. Carpineti, and A. Vailati, Phys. Rev. Lett. **85**, 1416 (2000).
[12] J. W. Goodman, *Speckle Phenomena in Optics* (Roberts & Company, Greenwood Village, CO, 2006).
[13] F. Ferri *et al.*, Phys. Rev. E **70**, 041405 (2004).
[14] R. Cerbino *et al.*, Nature Phys. **4**, 238 (2008).
[15] T. Narayanan, O. Diat, and P. Boesecke, Nucl. Instrum. Methods Phys. Res., Sect. A **467–468**, 1005 (2001).
[16] J. W. Goodman, *Statistical Optics* (Wiley-Interscience, New York, 2000), Chap. 5.
[17] R. N. Smartt and W. H. Steel, Jpn. J. Appl. Phys. **14**, 351 (1975).
[18] D. Magatti *et al.*, Appl. Phys. Lett. **92**, 241101 (2008).
[19] P. Cloetens *et al.*, Appl. Phys. Lett. **75**, 2912 (1999).
[20] M. Wu, G. Ahlers, and D. S. Cannell, Phys. Rev. Lett. **75**, 1743 (1995); F. Croccolo *et al.*, Appl. Opt. **45**, 2166 (2006).
[21] J. W. Goodman, in *Laser Speckle and Related Phenomena*, edited by J. D. Dainty (Springer-Verlag, Berlin, 1975).
[22] G. Geloni *et al.*, Nucl. Instrum. Methods Phys. Res., Sect. A **588**, 463 (2008). The vertical coherence length at the source can be calculated using Eqs. (58), (73), and (91).